Engineering Structures 270 (2022) 114867

Contents lists available at ScienceDirect

Engineering Structures

journal homepage: www.elsevier.com/locate/engstruct

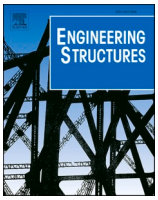

A holistic methodology for the non-destructive experimental characterization and reliability-based structural assessment of historical steel bridges

O. Bouzas *, B. Conde, M. Cabaleiro, B. Riveiro

CINTECX, Universidade de Vigo, GeoTECH Group, Campus Universitario de Vigo, As Lagoas, Marcosende, 36310 Vigo, Spain

ARTICLE INFO

Keywords:
Aging steel bridge
Non-destructive experimental testing
Model updating
Reliability analysis

ABSTRACT

Nowadays, several historical steel structures present damage and an advanced deterioration state induced by human or natural actions, causing fluctuations in geometrical, physical, and mechanical properties that dramatically affect their mechanical behavior. Due to the economic, cultural, and heritage value, these constructions must be comprehensively assessed to verify their current condition state. This work presents a holistic methodology aimed at the non-destructive experimental characterization and reliability-based structural assessment of historical steel bridges. It comprehends from the experimental data acquisition to the finite element model updating and the probabilistic-based structural assessment to obtain the reliability indexes of serviceability and ultimate limit states. Several sources of information are considered in the evaluation process, thus, results are more realistic and accurate and can be used for optimal decision-making related to maintenance and retrofitting actions. The feasibility of the methodology has been tested on O Barqueiro Bridge, an aging riveted bridge located in Galicia, Spain. The study first involved a comprehensive experimental campaign to characterize the bridge effectively at multiple levels: geometry, material, and structural system by the synergetic combination of different tools and methods: in-depth visual inspection, terrestrial laser scanner survey, ultrasonic testing, and ambient vibration test. Subsequently, a detailed FE model was developed and calibrated with an average relative error in frequencies of 2.04% and an average MAC value of 0.94. Finally, the reliability-based structural assessment was performed, yielding reliability indexes of 1.80 and 1.99 for the serviceability and ultimate limit states, respectively. Thus, the bridge could not withstand traffic loads with satisfactory structural performance in its current condition.

1. Introduction

Bridges are one of the most important assets within road and rail networks. They allow the connection and exchange of goods and culture between the different nucleus of population. Indeed, many ancient bridges are declared assets of cultural heritage, proclaiming their architectonical value and importance to society. Their collapse could lead to major civilian, cultural and economic losses; thus, preserving them is a priority in civil engineering. Nevertheless, many bridges suffer damage and advanced deterioration state caused by human actions, natural phenomena (e.g., corrosion), or increasing traffic demands. Furthermore, some of these structures surpassed the expected design service life and have not had suitable maintenance tasks for years, mainly due to budget constraints.

The structural assessment is a procedure that studies the mechanical behavior and the structural health of a given construction to evaluate its performance and integrity. The whole assessment process typically encompasses from the experimental characterization to the structural analysis. Regarding the former, in historical bridges, it is essential to avoid any alteration that could harm their heritage value. Therefore, as long as possible, non-destructive testing techniques should preferably be used to characterize the structure [1].

Historical steel bridges commonly present complex geometries. They are typically built up by different L-shaped steel profiles and plates joined by rivets. Besides, their dimensions might show variations due to the existing damages. Therefore, a combination of surveying techniques that can adequately capture all these issues must be used for proper geometrical characterization. Within this context, terrestrial laser

* Corresponding author.
E-mail address: oscar.bouzas.rodriguez@uvigo.es (O. Bouzas).

https://doi.org/10.1016/j.engstruct.2022.114867
Received 25 May 2022; Received in revised form 6 August 2022; Accepted 19 August 2022
Available online 5 September 2022

scanning has gained significant relevance over the last few years. This technique can measure the geometry of all the structural components in a short period providing thousands of measurement points that enables a reliable and accurate characterization of the geometry of the construction. The suitability of this technique has been demonstrated in numerous research works. Anigacz et al. [2] and Riveiro et al. [3] demonstrated the feasibility of the TLS systems to capture the global geometry of iron and masonry bridges, respectively. Kim et al. [4] and Yan et al. [5] have verified the TLS accuracy by extracting bridge segments and individual elements such as steel girders or cross-frames, among others. In Gyetvai et al. [6], researchers demonstrate how to extract the cross-sections of a bridge from a point cloud and how to generate a numerical model using these data. Concerning the physical and mechanical properties of the constituent materials, they are usually characterized by laboratory testing on specimens extracted from the structure. However, due to the non-intrusion requirement in historic bridges, non-destructive testing techniques should preferably be used instead. In this regard, elastic properties, namely the Young's modulus, might be estimated by analyzing the velocity of propagation of the sonic waves through the medium [7].

Developing a suitable and representative Finite Element (FE) model for a complex mechanical system such as an aging steel bridge is a challenging process. Thus, errors arise due to modeling simplifications when approximating the complex system behavior or uncertainties in input parameters, among other issues. This results in a discrepancy between numerical model predictions and actual measured responses from the structure. To bridge this gap, model updating or calibration techniques are employed, commonly using modal parameters (natural frequencies, mode shapes, and damping ratios) extracted from output-only modal analysis [8,9] as reference data. Model updating can be performed by manual means or automated methods. In this regard, Altunisik et al. [10,11] carried out two model updatings of real case studies using both approaches and comparing their results. Regarding automated calibration methods, two main methodologies can be distinguished: direct methods, which directly introduce modifications in the mass and stiffness matrices of the structural system to reproduce the experimental modal properties [12], and iterative methods that systematically modify model input parameters values aimed at minimizing some error measure that quantifies model discrepancies to the experimentally obtained modal properties. A considerable number of studies devoted to this issue can be found in the most recent literature, including global [13,14] and gradient-based optimization strategies [15,16], among others. Besides deterministic approaches, some authors have also used probabilistic methodologies such as Bayesian inference procedures for considering uncertainties in the model updating process [17].

As for structural assessment, deterministic or semi-probabilistic approaches using partial safety factors are widely used to assess the performance of a construction. Nevertheless, the experimental characterization process highlights the significant variability existing in the mechanical parameters of an aging structure. Therefore, assessment procedures based on these approaches might lead to inaccurate predictions wrongly estimating, e.g., the actual structure's load capacity. Thus, an assessment based on an approach that explicitly considers structural variables' uncertainty seems much more appropriate. Reliability analysis enables fulfilling this requirement by determining the probability of failure of a structure related to a given limit state. This way, a more trustworthy and accurate evaluation of the structure's condition can be obtained, leading to a more robust decision-making basis. This type of analysis has been widely adopted to assess civil engineering structures in the recent literature. In [18] authors performed a reliability analysis of a long-span arch bridge considering the variability of the loads acting on it. Kueres and Hegger [19] conducted a reliability-based assessment of a concrete footbridge to determine an appropriate safety factor for the CFRP tendons of the structure. Jamali et al. [20] and Matos et al. [21] used probabilistic analyses to evaluate concrete structures tested in the laboratory. In [22,23] Moreira et al. performed a probabilistic-based assessment of a masonry arch bridge considering inferential procedures. Conde et al. [24] conducted a reliability-based structural assessment of a historic stone arch bridge using a surrogate modelling strategy and two different numerical approaches: a three-dimensional non-linear finite element model and a two-dimensional rigid blocks limit analysis model. In Matos et al. [25], authors developed a framework to assess existing steel–concrete composite bridges, combining deterministic model updating and reliability-based assessment with Bayesian inference on a 2D plane stress FE model.

All the described stages (i.e., experimental characterization, model updating, and reliability-based structural assessment) improve the accuracy of numerical predictions and, consequently, the performance and ultimate load-carrying capacity evaluation of a structure. Thus, all stages should be appropriately linked to developing a robust methodology. Finite Element (FE) models can be solely based on literature data or partially supported by historical information (e.g., drawings). However, the structural assessment based on these models will most likely evaluate a theoretical scenario that departs from the actual condition of the construction. Non-calibrated numerical models could be employed in structural evaluations. However, there is no evidence that the numerical estimates suitably replicate the actual response of the structure. Finally, structural evaluations based on semi-probabilistic approaches are widely employed in civil engineering. Nevertheless, aging structures often present scattering in their mechanical properties that cannot be disregarded. In this case, these approaches could lead to misleading conclusions, being stochastic approaches more appropriate.

Many studies evaluate structural safety based on reliability approaches in the existing literature. Nonetheless, they did not integrate the model updating [22,23] or the experimental characterization [18,19] in their frameworks. In [20,21] the authors include all the stages mentioned above but on laboratory models, which allow the use of destructive testing techniques. Other studies [15,16] employ updated numerical models to evaluate structural safety within a deterministic or semi-probabilistic framework. In [26] all stages are addressed yet for assessing the fatigue response of railroad bridge components.

The main objective of this paper lies in proposing an integral and robust workflow that allows the reliability-based structural assessment of heritage civil engineering constructions, namely aging steel bridges. This holistic methodology encompasses all key stages (i.e., experimental characterization, model updating, probability-based structural analysis) to obtain an accurate evaluation and generate a reliable and valuable decision-making basis for optimizing the planning of retrofitting and maintenance actions. The feasibility of the methodology has been tested on a real case study, O Barqueiro Bridge, a historical riveted steel bridge located in Galicia, Spain.

2. Methodology

In Fig. 1, all steps of the proposed methodology are schematically outlined:

i. **Experimental characterization**. The construction is fully characterized by performing several different in-situ surveys. Only non-destructive testing techniques are employed to maintain the structure's condition intact. Hand-made measurements, 3D digitalization through terrestrial laser scanning, ultrasonic tests, and ambient vibration test results are collected and processed to obtain experimental data exploited in posterior stages. Additionally, a comprehensive visual inspection is conducted to identify existing construction damages, magnitude, and location.
ii. **Numerical modeling.** Based on all the previously collected information, a detailed 3D Finite Element (FE) model that appropriately replicates the physics of the construction is developed.
iii. **Uncertainty quantification**. During this stage, literature and experimental data are analyzed to define the statistical distributions for the uncertain parameters.

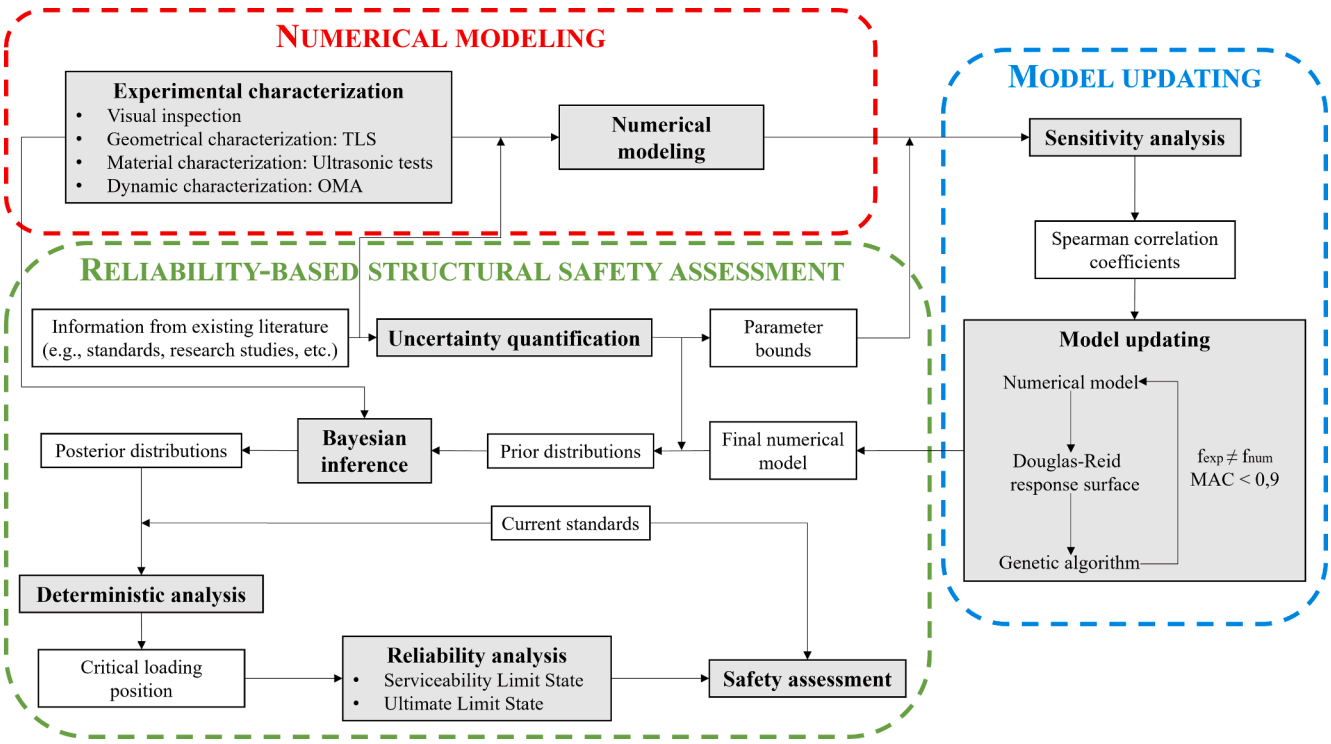

Fig. 1. Flowchart of the proposed methodology.

iv. **Sensitivity analysis.** Sensitivity analysis determines the most influential model input parameters in the output responses, allowing disregarding the non-influential during the optimization process. This results in both improved efficiency and identifiability.

v. **Model updating.** Model calibration allows for a reliable simulation model that correctly resembles the actual bridge's mechanical behavior. The Douglas-Reid (DR) method, in combination with a global optimizer, a genetic algorithm, is adopted to minimize an error function that quantifies the discrepancies between numerical and experimental modal properties.

vi. **Bayesian inference**. Bayesian inference is used to incorporate experimental data in the numerical model updating the probability distributions of the structural parameters. Prior distributions are defined based on the model updating results, data from the literature, experience, and engineering judgment. These probabilistic distribution laws are then updated with the experimental data collected during the characterization campaigns to yield the posterior distributions.

vii. **Deterministic analysis.** Once the model is calibrated, a deterministic analysis is carried out to find the most unfavorable section of the structure,.i.e, the critical loading position.

viii. **Reliability analysis.** The probability of failure and the reliability index of the structure are calculated for several limit states, such as the serviceability limit state affecting the structure's functionality and the ultimate limit state related to the collapse of the structure.

ix. **Safety assessment.** All previous results are discussed and compared with the target values imposed by current standards. Thus, conclusions regarding the functionality and safety of the structure are drawn, which are vital for correctly scheduling maintenance and retrofitting actions.

3. O Barqueiro bridge

3.1. Historical background

O Barqueiro Bridge, located in Galicia, northwest of Spain, is a riveted steel arch bridge that crosses the Sor river, linking the municipalities of O Mañón, in the province of A Coruña, and Vicedo, in Lugo. O Barqueiro Bridge greatly impacted society because it allowed the crossing of people and goods between the two regions. Before its construction, inhabitants had to use boats to cross the estuary.

The first project dates from 1880. Nevertheless, its construction did not start until 1895, finally opening in 1901. O Barqueiro Bridge is in a harmful atmosphere due to the high concentration of saltpeter in the air. Thus, it has been exposed to deterioration due to corrosion throughout its service life. This issue led to a restriction on vehicle passage in 1980 because of the damage present in the construction. Years later, the structure was closed entirely. In 2006, the Galician regional government earmarked 1.2 million euros for the rehabilitation of the bridge. This intervention enclosed the repair of the damaged elements and the pedestrianization of the structure.

Nowadays, O Barqueiro Bridge is declared an asset of cultural interest in Galicia, which officially proclaims its heritage value and its repercussion on the life of the inhabitants of the area. This fact largely justifies the importance of its correct maintenance and monitoring of its structural health.

3.2. Description of the bridge

O Barqueiro Bridge is a three-isostatic-span riveted steel arch bridge (Fig. 2). Each span has a length of 48.1 m, comprising thirteen panels of 3.70 m long, a maximum height of 7.5 m, and a width of 6.4 m (Fig. 3 (a) and (b)). All original bridge elements are built-up members of different steel plates and L-type profiles (Fig. 4 and Table 1), initially connected by rivets and now partially substituted by bolts and welding in a few locations.

The arch rib and the tie girder were built using I-shaped sections

Fig. 2. Overall view of O Barqueiro Bridge.

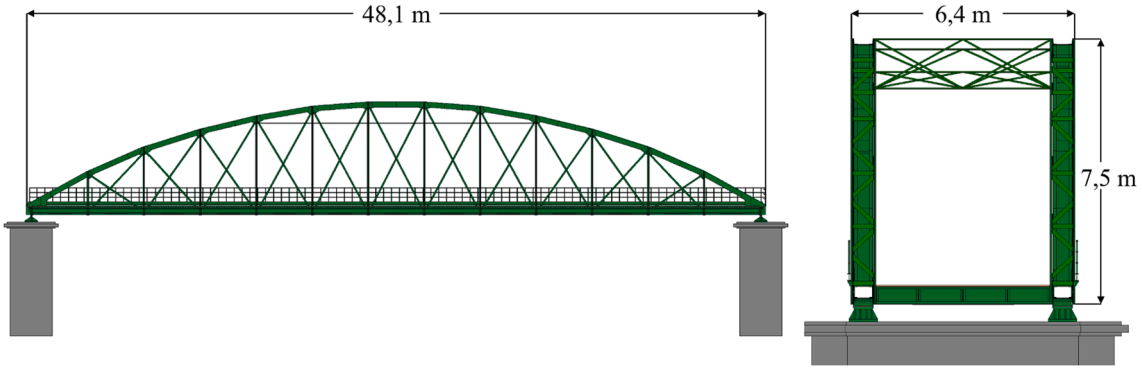

Fig. 3. O Barqueiro Bridge: (a) lateral view and (b) cross-section.

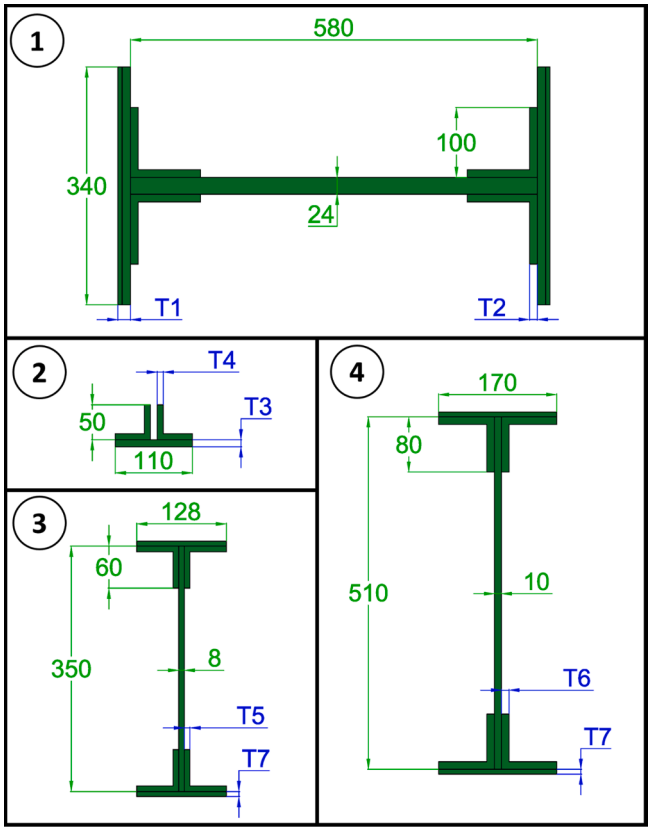

Fig. 4. Cross-section of steel members.

Table 1
Statistical data of the thickness measurements.

ID	Parameter	Mean (mm)	Standard deviation (mm)	Maximum (mm)	Minimum (mm)
T1	Arch/girder flange thickness	17.67	0.40	18.70	16.98
T2	Arch/girder L-shaped profile thickness	10.73	0.68	12.11	9.02
T3	Vertical hanger plate thickness	8.98	0.92	10.83	7.18
T4	Vertical hanger L-shaped profile thickness	8.20	0.61	9.59	6.79
T5	Stringer L-shaped profile thickness	7.23	1.45	8.96	2.90
T6	Crossbeam L-shaped profile thickness	10.83	0.58	11.9	9.57
T7	Reinforcement plate thickness	7.50	0.87	8.89	6.18

(Fig. 4, section 1), being connected through twenty-four vertical hangers. The hangers are formed by pairs of double angles and a support plate (Fig. 4, section 2), transversally connected by lacings, and longitudinally by rectangular-shaped cross bracings. Twelve sway systems, with struts made of double angles and rectangular-shaped bracings, connect both arch ribs, providing lateral stiffness to the structure. Sway systems are, in turn, longitudinally connected by circular-shaped upper lateral bracings.

The bridge's deck comprises sixty-five stringers equally divided into five rows. These members are joined to fourteen crossbeams, which are in turn linked to the tie girders and vertical hangers. The stringers and crossbeams are I-shaped (Fig. 4, sections 3 and 4, respectively). All the

crossbeams and central stringers have two reinforcement steel plates on the top and bottom sides to increase flexural capacity. Several circular-shaped lower lateral bracings connect the crossbeams longitudinally. Moreover, after rehabilitation, the original road pavement was replaced by rectangular wooden planks. Fig. 3(b) shows the bridge cross-section, while Fig. 5 provides some details about the actual structural configuration.

3.3. Visual inspection

Before the experimental campaign, a thorough visual inspection was carried out to evaluate the conservation state of the bridge, especially for having a depth insight into the severity and corrosion extension in the different steel elements. Accordingly, a damage mapping was elaborated together with identifying, examining, and assessing the retrofitting actions performed during the rehabilitation.

The bridge presents corrosion in almost all its elements, caused by the high concentration of saltpeter in its location, although, in general terms, this corrosion might be regarded as primary uniform. The exceptions are local areas where dimples and holes can be found and some steel connections between crossbeams, vertical hangers, and tie girders. Most corroded elements are located at the bridge parts where the moisture, water, and saltpeter remain for a long time, such as in the stringers and crossbeams due to the contact with the timber deck, and the arch ribs and tie girders, where organic residues are deposited (see Figs. 5 and 7).

As for the steel connections, some have experimented a substantial degradation as they present elements with an important lack of material or a lack of enough connectivity due to the absence of rivets. Thus, each connection was individually inspected during the on-site survey, and a qualitative classification was elaborated, attending to their damaged state. The steel connections were clustered into two major categories: a) slightly damaged connections, i.e., those presenting minor to moderate material losses at the structural members, and b) highly damaged connections, i.e., those with some of their elements significantly corroded. This classification is schematically shown in Fig. 6.

On the other hand, the mechanical behavior of bridge structural elements was also inspected. Thus, it was observed that the connection between stringers and crossbeams can be regarded as pinned, allowing the in-plane rotation of the stringers (see Fig. 7). On each span, the girders are supported by pin bearings on one side and roller bearings on the other, with no interaction between spans (see Fig. 7). Moreover, it was verified that each span presents the same type and arrangement of structural components with the same shape and dimensions of their cross-sections. Hence, once the isostatic behavior of each span was verified, the experimental and numerical studies were focused on a single span to minimize experimental and computational costs.

Finally, the retrofitting works were observed. During the rehabilitation performed in 2006, the structure was painted for aesthetic and protection purposes. Besides, several rivets were replaced by bolts, and twenty-six cross-bracings and twelve vertical hangers were retrofitted or replaced. Indeed, new L-type sections were employed, which were connected to the old steel plates by welding instead of bolts. Remarkably, the vertical hangers that were joined by welding present a more severe corrosion state than the other hangers in the bridge. A brief detailing of all these issues can be observed in Fig. 7.

4. Experimental characterization

4.1. Geometrical characterization

Historic steel structures often exhibit a complex geometry due to the large number of elements that make them up. Moreover, usually, design drawings do not exist, or even if they exist, they might not represent the final aspect due to design modifications introduced in the construction phase. To create an accurate structural model, detailed and precise information about the bridge geometry is needed. Over the last years, this requirement has been satisfactorily addressed using Terrestrial Laser Scanner (TLS) technology and photogrammetry techniques. Particularly, the TLS is widely used in the architecture and civil engineering field for capturing thousands of measuring points in a short period providing an accurate 3D digitalization of the construction.

Since, in the case of O Barqueiro Bridge, almost no information on the geometry of the construction was available on existing documentation, aside from very scarce information related to the length of the spans and deck width, this study conducted a laser scanning survey employing the FARO Focus 3D x130 scanner (see Fig. 8). During the data acquisition stage, several targets were placed along the whole bridge to

Fig. 5. Details of O Barqueiro Bridge: (1) arch rib (2) vertical hanger (3) stringers (4) sway systems (5) crossbeams.

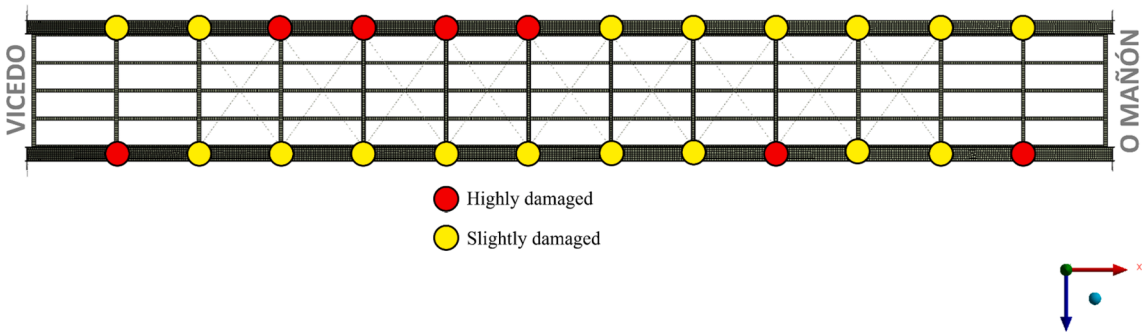

Fig. 6. Scheme of the damaged condition state of the steel connections.

Fig. 7. Details of the current condition state of the bridge: (1) simple support and the gap between spans (2) connection between stringers and crossbeams (3) lack of rivets in a stringer (4) heavily corroded retrofitted vertical hanger (5) corrosion in a crossbeam.

ease the posterior registration in a common coordinate system of all laser scans. Ten scan positions were recorded, six on the deck and four under the bridge (see Fig. 9). All laser scans were post-processed in the CloudCompare software [27]. A final point cloud comprising 12,431,238 points was obtained, which provided a detailed geometric description in the form of an "as-built" model that renders information not only about the overall geometry but also regarding the type and dimensions of steel profiles and their assembly. Furthermore, in the case of high-density laser scans, the associated point cloud can be additionally used to cross-check the cross-section dimensions of steel members.

Additionally, on-site hand measurements were collected aimed at characterizing the net cross-section of the steel members and quantifying the scattering related to the thickness dimensions. A precision gauge with a tolerance of $\pm$ 0.01 mm was employed to obtain a total of 325 values spread over the main members (stringers, vertical hangers, tie girders, etc.) and on different regions (i.e., L-shaped profiles and steel plates). The statistical data of these measurements are shown in Table 1, displaying the thicknesses variability due to its inherent uncertainty and the corrosion affection.

4.2. Material characterization

Even though the whole bridge is made of structural steel, deviations in mechanical properties might appear because of its inherent variability and the deterioration condition of the bridge. Usually, the physical and mechanical properties of the constituent materials of a construction are characterized by laboratory testing, such as uniaxial tensile tests that involve the extraction of specimens from the structure. However, these are destructive tests that alter the original state of the construction. Since the methodology herein proposed is aimed at historic bridges, which usually have a significant cultural and heritage value, and where the non-intrusion requirement is a constraint to be satisfied, this

Fig. 8. Geometry data acquisition using Terrestrial Laser Scanner (TLS) technology.

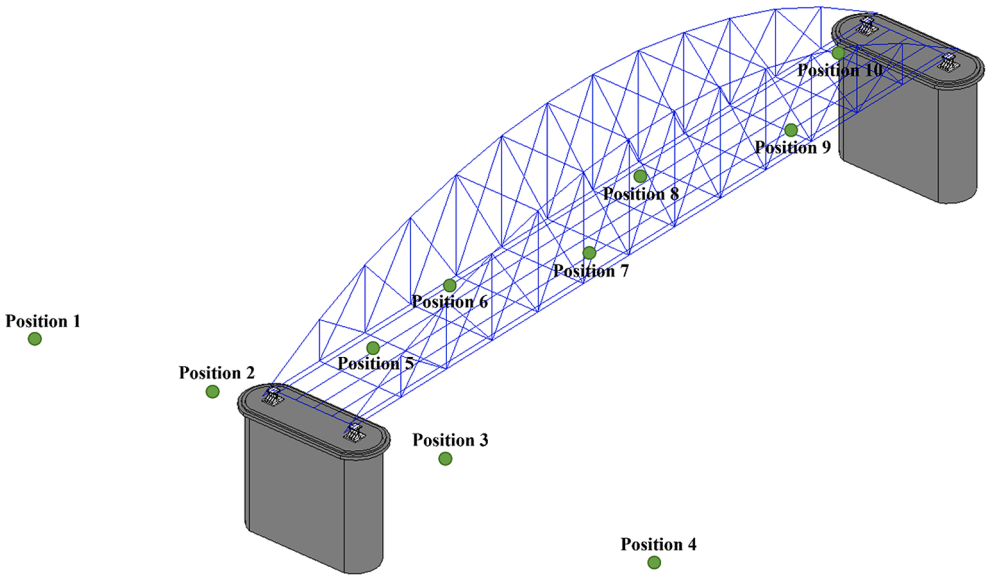

Fig. 9. Scheme of laser scan positions.

research adopted a non-destructive in-situ testing technique, an ultrasonic test, to estimate these data, namely the Young's modulus.

There is a relationship between the velocity of propagation of transversal waves C_t through a steel element and its Young's modulus E. This is represented in the following equation, where μ and ρ are the Poisson's ratio and the density of the material, respectively.

$$E = 2 \bullet \rho \bullet C_t^2 \bullet (1 + \mu) \tag{1}$$

Hence, it is possible to characterize the Young's modulus according to the following procedure. Firstly, the thickness of a tested area is measured using an ultrasonic thickness gauge. In this study, the MX-3 equipment of Dakota Ultrasonics was used. Subsequently, the same thickness is measured again using a high-precision digital gauge (see Fig. 10). Finally, the first measurement is corrected in the ultrasonic device, which returns the velocity of propagation of the longitudinal waves C_l.

In Equation (1), the Young's modulus is related to the velocity of the transversal waves C_t. Both velocities are related by the Poisson's ratio, as represented in Equation (2). Combining Equations (1) and (2), Equation (3) that relates the Young's modulus of the material and the velocity of propagation of the longitudinal waves can be finally obtained.

Fig. 10. Ultrasonic testing: measurement of the velocity of propagation of the longitudinal waves.

$$\mu = \frac{\left(\frac{1}{2}\right) - \left(\frac{C_t}{C_l}\right)^2}{1 - \left(\frac{C_t}{C_l}\right)^2} \tag{2}$$

$$E = \rho \bullet C_l^2 \bullet (1+\mu) \bullet \frac{1-2\bullet\mu}{1-\mu} \tag{3}$$

During the experimental campaign, a total of 66 tested areas were measured. In each position, the described procedure was repeated five times. The final post-processed data yielded a Young's modulus with a mean value of 188.94 GPa and a standard deviation of 9.90 GPa. The maximum and minimum values were 224.28 GPa and 173.46 GPa, respectively.

4.3. Dynamic characterization

Operational Modal Analysis (OMA) is a well-known non-destructive testing technique to obtain the modal parameters of a structure (i.e., natural frequencies, mode shapes, and damping ratios). This technique is based on ambient vibration testing, where the vibration response of the structure is measured under ambient excitation sources such as wind and traffic actions, being an efficient and effective characterization technique. Hence, many researchers have employed output-only modal analysis over the last few years to characterize the dynamic response of in-service constructions.

This work used six uniaxial seismic accelerometers type 8340 of Brüel & Kjaer to perform the ambient vibration test (see Fig. 11). These accelerometers have a sensitivity of 10 V/g and a frequency range of 0.1–1500 Hz. A multi-setup test was adopted where the location of the sensors was mainly driven by the constraints in the number of available accelerometers and the lengths of the cables so as to cover the whole bridge geometry satisfactorily. Consequently, the adopted positions were targeted to those areas with non-zero modal displacements. In this sense, the outcomes of several numerical simulations performed with a preliminary FE model were considered to establish the main conditions of the test (acquisition time, sampling rate, and location of the sensors). The test consisted of twenty-one setups involving forty-three accelerometer positions and using two reference sensors (see Fig. 12). Ad-hoc steel supports connected to magnetic anchors were used to fix the accelerometers to the tie girders and vertical hangers. In each setup, accelerations in vertical and transversal directions were recorded. A sampling frequency of 128 Hz and an acquisition time of 45 min were adopted. During the dynamic test, the structure was subjected to environmental and operational loads such as wind and human traffic.

Modal properties were extracted using the Enhanced Frequency Domain Decomposition (EFDD) and the Stochastic Subspace Identification (SSI) methods in the Artemis software, see Table 2. A total of four natural frequencies were identified, ranging from 1.05 Hz to 7.36 Hz. Generally, there is a good agreement between the natural frequencies but a higher discrepancy between the damping ratios [28]. The first vibration mode is a symmetric flexural mode shape in the transversal (Z-axis) direction, while the second vibration mode corresponds to an asymmetric flexural mode shape between the arch and the deck in the transversal (Z-axis) direction. On the other hand, the third vibration mode is a vertical (Y-axis) flexural mode shape of the whole structure, while the fourth is a torsional mode shape. The identified vibration modes are shown in Fig. 13.

5. Numerical modeling

5.1. Model development

The data gathered from the experimental characterization tests were used to build a numerical model that accurately represents the structural behavior of the bridge. The as-built CAD model was created based on the TLS point clouds and the on-site manual measurements. 3D line bodies were employed to model most of the bridge elements except for the arch ribs and tie girders, which were modeled using line bodies for the flanges and surface bodies for the webs.

The Finite Element (FE) model was developed in the ANSYS software package (see Fig. 14). The vertical hangers, crossbeams, and stringers were meshed by using second-order Timoshenko beam elements. For the cross bracings, since a stress-stiffening response is expected, they were modeled as tension-only two-node truss elements. For the arch ribs and tie girders, a mixed modeling approach was adopted where second-order quadrilateral isoparametric shell elements were used for the webs and second-order Timoshenko beam elements for the L-shaped flanges. In all cases, the complex shapes of the cross-sections of the beam elements were defined based on the experimental geometrical characterization (see Fig. 4). For the resulting arbitrary cross-section types, the cross-sectional analysis was performed via the Finite Element Method (FEM) in order to obtain the warping independent and dependent properties. It is worthwhile to note that the actual position of the centers of gravity of the beam elements was accounted for by using suitable offsets from the supporting CAD axes (see details in Fig. 14). The mesh size of the FE model was derived from a sensitivity analysis aimed at guaranteeing an equilibrium between computational efficiency and accuracy. In this regard, a total of 11,667 beam elements, 140 truss elements, 11,412 shell elements, 70 beam end releases, 24 rotational springs, and 8 translational springs were employed.

Regarding the joints, most of the beam elements were connected by rigid link types except for the connections between the stringers and the crossbeams, where end releases were introduced to allow in-plane

Fig. 11. Accelerometers placed on the tie girder and a vertical hanger.

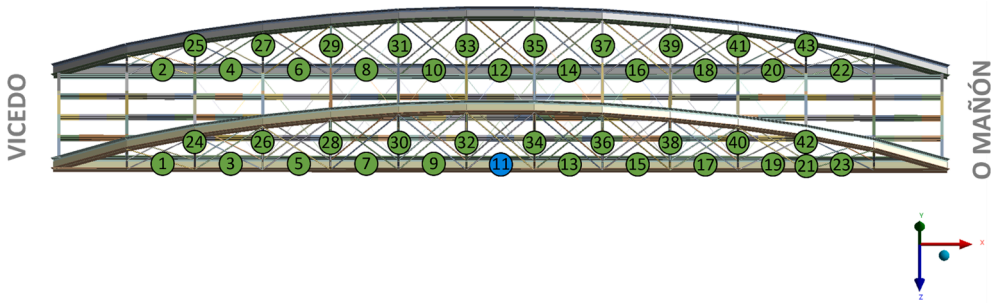

Fig. 12. Schematic representation of the accelerometer positions in the ambient vibration test. In blue are the reference sensors, and in green are the roving sensors. (For interpretation of the references to colour in this figure legend, the reader is referred to the web version of this article.)

Table 2
Experimental modal parameters of O Barqueiro Bridge.

Mode	Frequency (Hz)		Damping ratios (%)	
	SSI	EFDD	SSI	EFDD
1	1.05	1.07	1.36	1.64
2	2.71	2.71	1.63	1.66
3	6.19	6.19	2.59	0.51
4	7.36	7.34	1.37	0.61

rotations of the stringers. Two different criteria were adopted for the main bridge connections, i.e., those involving vertical hangers, crossbeams, and tie girders. According to the visual inspection (see Fig. 7), pinned joints were assumed for the highly damaged connections, thus disregarding any bending moment capacity; while for the slightly damaged connections, rotational springs were introduced to allow the modeling of a semirigid behavior. On the other hand, regarding the contribution of other bridge components, the timber deck was introduced in the model as a dead load distributed on the crossbeams and stringers, assuming a density of 500 kg/m3, while the mass of the gusset plates was considered in the form of point masses acting at the different joints.

As for boundary conditions, at the O Mañón side (see Fig. 6), in-plane (Z-axis) rotations were permitted. At the O Vicedo side, both displacements in the longitudinal (X-axis) direction and in-plane (Z-axis) rotations were allowed. In addition, to consider the deformability of the supports, translational springs in the vertical (Y-axis) and transversal (Z-axis) directions were introduced in the numerical model. Finally, regarding the steel material properties, the estimates obtained from ultrasonic testing were used as the initial value for the Young's modulus together with a density of 7850 kg/m3 and a Poisson's ratio of 0.3. Table 4 summarizes all the main geometrical and mechanical parameters of the FE model.

A pres-stress modal analysis using the self-weight of the structure was carried out due to the geometric non-linearity (stress-stiffening response) of the bracing systems. Numerical and experimental responses were compared using the relative differences in frequencies and the Modal Assurance Criterion (MAC) [29]. The results obtained are shown in Table 3. Regarding the mode shapes, it was observed that numerical and experimental modal displacements agreed well. Indeed, the MAC values were equal to or above 0.95. Nevertheless, discrepancies between the numerical and experimental frequencies were observed, especially in the first natural frequency. Hence, the need for FE model updating is highlighted in order to achieve a better correlation.

5.2. Model calibration

In this study, an automatic iterative calibration method was used. MATLAB and Phyton codes were developed to automatize all the model calibration stages, from the updating of parameters to the comparison between numerical and experimental dynamic responses. These codes start by generating the Design of Experiments (DoE), i.e., by sampling the input parameters' space. Once the material properties, stiffness, and thicknesses values are updated, the structural elements' cross-section properties are calculated by a Python code, which creates a quadratic mesh in each cross-section and obtains the area, the second moments of area, and the torsional and warping constants by numerical integration [30]. Subsequently, the code automatically introduces the parameter values in the input data file of the solver and runs the numerical analysis

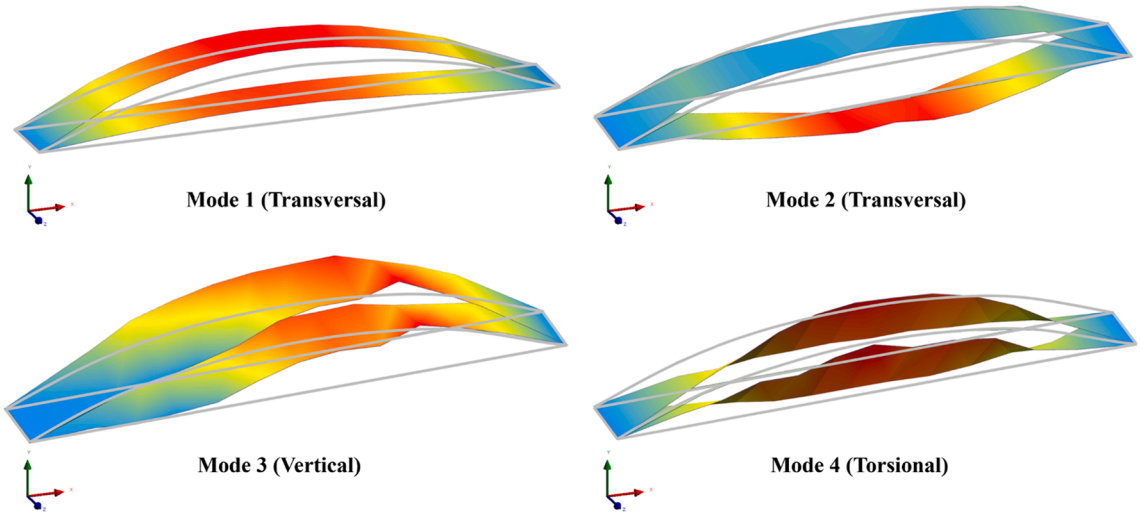

Fig. 13. Vibration modes obtained from the OMA test.

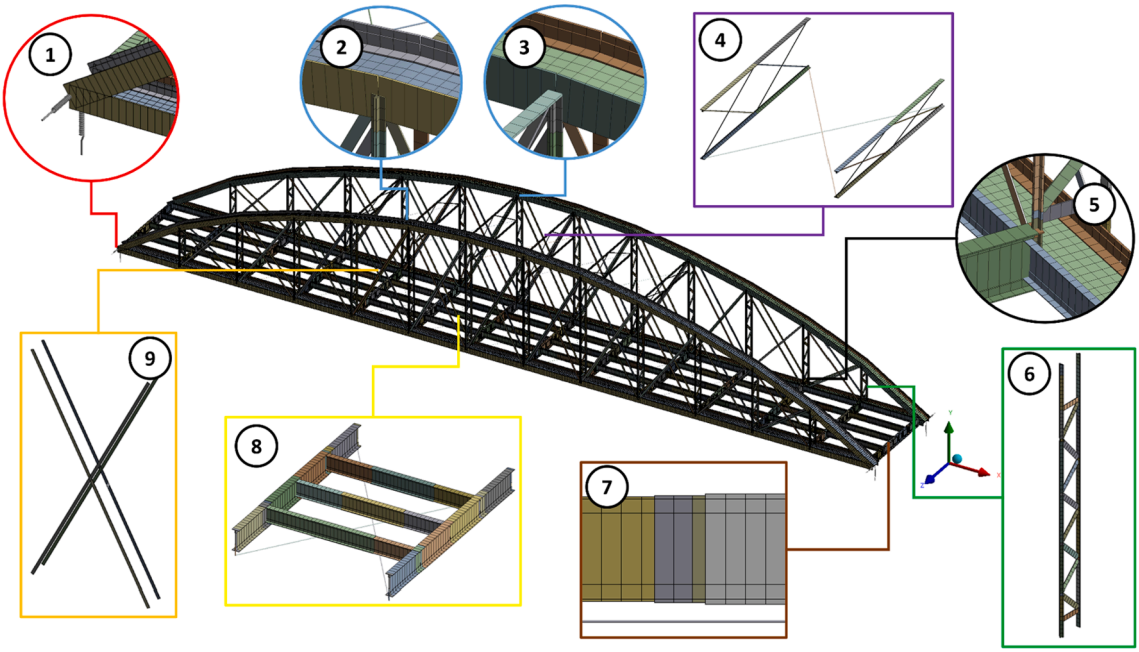

Fig. 14. FE model of O Barqueiro bridge.

Table 3
Comparison of experimental and numerical results for the initial (non-calibrated) FE model.

Mode	Experimental	FE model		
	Frequencies (Hz)	Frequencies (Hz)	Frequency error (%)	MAC
1	1.05	1.48	41.04	0.97
2	2.71	2.61	3.95	0.97
3	6.19	6.30	1.74	0.95
4	7.36	7.28	1.17	0.95

Table 4
Parameters considered in the model calibration process.

ID	Parameter	Initial value	Lower Bound	Upper Bound	Units
V1	Density	7850	7614.50	8085.50	kg/m^3
V2	Young's modulus	188.94	172	232	GPa
V3	Arch ribs/tie girders	0	−4.64	0	mm
V4	Vertical hangers	0	−4.64	0	mm
V5	Stringers	0	−4.64	0	mm
V6	Crossbeams	0	−4.64	0	mm
V7	Reinforcement plates	0	−4.64	0	mm
V8	Rotational stiffnesses of slightly damaged connections	1.00E + 07	100	1.00E + 07	N•m/rad
V9	Translational stiffnesses of Vicedo support (Y-axis)	5.01E + 10	1.00E + 08	1.00E + 11	N/m
V10	Translational stiffnesses of O Mañón support (Y-axis)	5.01E + 10	1.00E + 08	1.00E + 11	N/m
V11	Translational stiffnesses of Vicedo support (Z-axis)	5.01E + 07	1.00E + 05	1.00E + 08	N/m
V12	Translational stiffnesses of O Mañón support (Z-axis)	5.01E + 07	1.00E + 05	1.00E + 08	N/m

in batch mode. Finally, the modal properties are compared with the experimental ones, quantifying the frequency error and MAC values. In this regard, the automatic mode pairing between numerical and experimental vibration modes was based on both the MAC criterion and the assessment of modal masses to dismiss local mode shapes. This code was run during the sensitivity analysis and the model calibration process.

5.2.1. *Parameter ranges*

The parameter bounds were defined based on existing literature such as standards, research studies, and the collected experimental data. Concerning the material properties, in the JCSS standard [31], the variability of the structural steel density is defined as a Gaussian distribution with a CoV of 1 %. Consequently, the three-sigma rule of thumb was applied, and the selected bounds were the values that delimit a confidence interval of 99.7 %. On the other hand, previous research works defined the variability of Young's modulus as a log-normal distribution with a CoV of 5 % [32]. Similarly, based on the inverse cumulative distribution function, the selected bounds were the ones that define a confidence interval of 99.7 %.

Regarding the geometrical properties, it is worth noting that, despite the significant amount of measurements collected, these are still discrete and discontinuous. Therefore, uncertainty regarding the actual geometrical dimensions remains. This uncertainty comes from both its inherent variability and the added corrosion affection due to the spatial variation of the phenomenon. Initially, the average experimental measurements for the cross-sections' dimensions were used (see Fig. 4 and Table 1). Since there is uncertainty regarding geometrical dimensions, namely members thicknesses, these variables were considered during the sensitivity analysis and the model updating process. The upper bound value was defined as the average experimental measurements, i.e., the initial value. The lower bound value was defined as the average experimental measurements minus the maximum theoretical corroded thickness according to the existing standards dealing with the corrosive deterioration in steel [33,34]. These state that the average corrosion rate can be obtained by defining the corrosivity category of the atmosphere where the structure is located, which is described by the wetness and the concentrations of SO2 and chlorides in the air. O Barqueiro bridge is situated in a coastal area, i.e., a C5 corrosivity area. Therefore, given its service life, the corresponding corrosion rate was 39 μm/year, leading to a maximum theoretical corroded thickness of 4.64 mm. Since the average experimental measurements have already considered the net cross-section, these variation ranges should be interpreted herein more within the context of defining a sufficiently large parameter space, with a reasonable support basis, to study the influence of uncertainty in geometrical dimensions (i.e., thicknesses) on the structural mass and stiffness (and thus on modal responses) rather than an actual corrosion

scenario. Accordingly, for model updating purposes, the geometrical calibration parameters were defined as a factor of perturbation of the base thickness values instead of the many non-identifiable individual dimensions.

Finally, with regards to the stiffness of the slightly damaged connections between vertical hangers, crossbeams, and tie girders (see Fig. 6), the selected bounds delimit a semirigid response, i.e., beyond the upper bound, the connection behaves as fully rigid, and below the lower bound as pinned. As for the stiffness of the supports, a similar approach was followed, where the upper bound value corresponded to fully constrained displacements, and the lower bound was delimited by observing the minimum stiffness value that guaranteed that all the experimental vibration modes could be captured. All parameters and their variation ranges are shown in Table 4.

5.2.2. Sensitivity analysis

Before model calibration, a sensitivity analysis was performed to distinguish between influential and non-influential parameters on the dynamic behavior of the bridge. This allows further insight into the mechanical response of the structure. Besides, sensitivity analysis outcomes are of particular value to ensure adequate identifiability and enhance the efficiency of the subsequent optimization process.

The method of Spearman correlation coefficients was adopted. This method is characterized by its simplicity and generality since it is applicable regardless of the dependence between variables [35]. The Spearman correlation coefficients adopt values in the interval [-1, 1]; one indicates a strong positive correlation, and minus one a strong negative correlation.

The parameters of Table 4 were analyzed to evaluate their influence in a total of eight numerical responses (frequency and MAC values). Initially, 100 samples were generated based on Sobol's sequences. Subsequently, the model responses were calculated, and the matrix of Spearman correlation coefficients was built. This process was repeated iteratively by increasing the number of samples (100 in each iteration) until the Spearman correlation coefficients showed no significant changes from one iteration to the next.

Fig. 15 shows the final matrix of Spearman correlation coefficients, obtained after considering a total number of 600 samples. The parameters in the interval [-0.25; 0.25] were deemed non-influential, and thus, their values were fixed at the initial ones (see Table 4). On the contrary, the correlation matrix shows that Young's modulus of the material, the thickness dimensions of the arch ribs and vertical hangers, the rotational stiffness of the slightly damaged steel connections, and the supports' translational stiffness in the transversal direction are the most influential parameters into the bridge modal responses. Hence, all of them were considered in the following model calibration process.

5.2.3. Douglas-Reid approach

The model calibration consisted of the minimization of the objective function $\pi(\boldsymbol{x})$:

$$\pi(\boldsymbol{x}) = \sum_{i=1}^{m} w_i \varepsilon_i^2 \tag{4}$$

$$\varepsilon_i = f_{i,exp} - f_{i,num}(\boldsymbol{x}) \tag{5}$$

where $f_{i,exp}$ and $f_{i,num}(\boldsymbol{x})$ are the i-th experimental and numerical frequency, respectively, $\boldsymbol{x}$ is the vector of calibration parameters, w_i are suitable weighting factors, and m denotes the number of frequencies considered in the updating process.

A response-surface method was adopted to solve the optimization problem, particularly the Douglas-Reid approach. This methodology replaces the time-consuming numerical model responses $f_{i,num}(\boldsymbol{x})$ with faster approximation models $f_i^*(\boldsymbol{x})$ based on second-order polynomial functions. Thus, considerable reductions in terms of time and computational costs are obtained when solving the parameter identification problem, especially if global optimization algorithms such as, e.g. genetic algorithms are employed. The polynomial functions are calculated according to Equation (6) [36].

$$f_i^*(x_1, x_2, \cdots, x_n) = \sum_{k=1}^{n} \left(A_{ik} x_k + B_{ik} x_k^2\right) + C_i \tag{6}$$

where f_i^* denotes the approximated i-th eigenfrequency of the numerical model, $x_k (k = 1, 2, \cdots, n)$ are the calibration parameters and A_{ik}, B_{ik} and C_i are the coefficients of the second-order function. These constants can be calculated from a system of equations of $2n+1$ elements, as shown in Equation (7), where n represents the total number of variables.

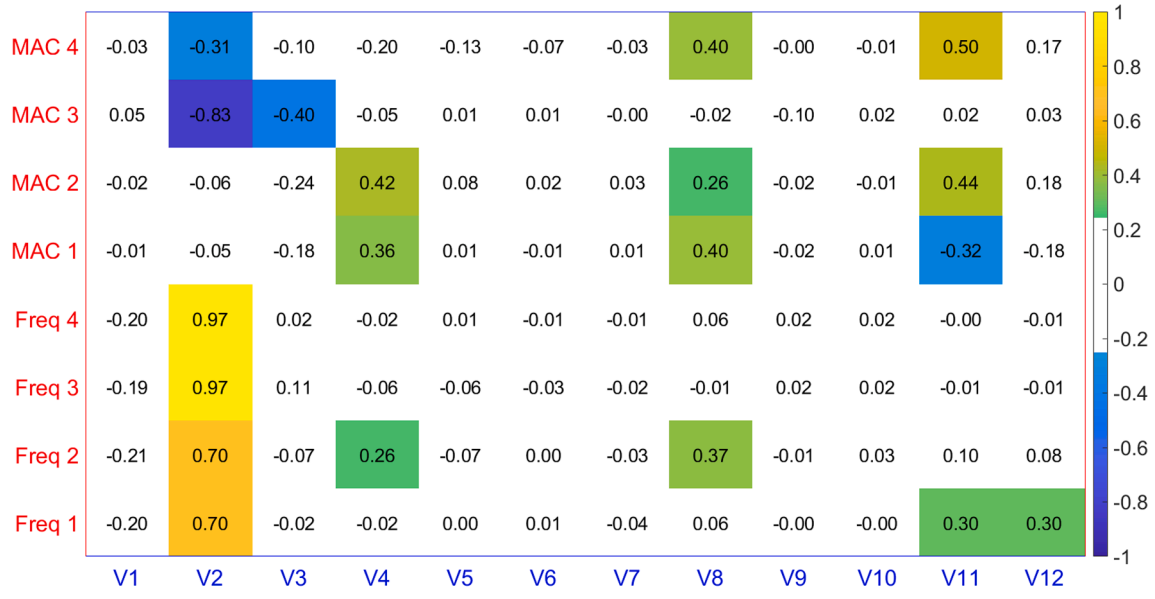

Fig. 15. Matrix of Spearman correlation coefficients relating input parameters to output responses.

$$\begin{cases} f_i^{num}(x_1^B, x_2^B, \cdots, x_n^B) = f_i^*(x_1^B, x_2^B, \cdots, x_n^B) \\ f_i^{num}(x_1^L, x_2^B, \cdots, x_n^B) = f_i^*(x_1^L, x_2^B, \cdots, x_n^B) \\ f_i^{num}(x_1^U, x_2^B, \cdots, x_n^B) = f_i^*(x_1^U, x_2^B, \cdots, x_n^B) \\ \vdots \\ f_i^{num}(x_1^B, x_2^B, \cdots, x_n^L) = f_i^*(x_1^B, x_2^B, \cdots, x_n^L) \\ f_i^{num}(x_1^B, x_2^B, \cdots, x_n^U) = f_i^*(x_1^B, x_2^B, \cdots, x_n^U) \end{cases} \quad (7)$$

The superscripts B, L, and U are referred to as the base, lower, and upper bound values of the parameters. In the Douglas-Reid methodology, a proper selection of these points is crucial for a good approximation. In its standard implementation, the base values correspond to user-selected values based on experience or appropriate engineering judgment.

In this study, on the contrary, the results obtained in the sensitivity analysis were exploited for an optimal choice of the base values. Thus, sampling results related to the scanning of the multidimensional space of the model parameters were further post-processed, and the set of parameter values with the lowest total error, i.e., considering the lowest frequency errors and the highest MAC values, were selected as base values for building the Douglas-Reid response surface model.

Subsequently, a genetic algorithm was used to minimize the objective function of Equation (4). Five independent optimization runs with different initial populations were carried out. The initial population consisted of 100 individuals created by a uniform Latin Hypercube sampling. Out of these 100 individuals, the five with the best fitness values were automatically passed to the next generation (elitism). The fraction of new individuals created by crossover was 70 %, and the remaining percentage was assigned to mutation. The algorithm was run for a maximum of 200 generations.

The optimization results presented in Fig. 16 show the parameter values received from the different genetic algorithm runs, normalized between 0 (lower bound) and 1 (upper bound). Table 5 shows the actual calibrated values for the best optimization run (i.e., the fifth), and Table 6 reports the dynamic response predictions. Finally, the numerical mode shapes of the calibrated FE model are depicted in Fig. 17.

The Young's modulus obtained indicates a global deterioration of the steel members due to the aging of the structure, presenting a good agreement with the estimations derived from the ultrasonic tests. On the other side, the calibrated values for the thicknesses of the arch ribs and vertical hangers remained unchanged, indicating a reasonable estimation in the contribution to the overall stiffness and mass of the bridge when adopting the average experimental measurements. Finally, calibration results suggest a significant rotational stiffness for the slightly damaged steel connections. This is in line with previous research findings [9,14] which point out the fact that for low excitation levels, as in the case of ambient vibration testing, bridge supports and connections might experience reduced displacements and rotations, thus behaving as almost fully rigid, differently that under high-intensity loads such as traffic actions.

Table 5
Parameter values obtained after model calibration.

Parameter	Normalized value	Actual value
V2	0.19	184 GPa
V3	1.00	0.00 mm
V4	1.00	0.00 mm
V8	0.91	9.11E + 06 N•m/rad
V11	0.01	5.20E + 05 N/m
V12	0.24	2.40E + 07 N/m

The calibrated FE model shows an important improvement in frequency errors. The gap between the actual and calculated frequencies has been substantially reduced, having all vibration modes a discrepancy lower than 5 %. On the other hand, all MAC values are higher than 0.90, being the average value above 0.94. Hence, a good correlation between numerical and experimental mode shapes was also achieved.

6. Reliability-based structural safety assessment

6.1. Uncertainty quantification

For a reliable structural system performance evaluation, uncertainties in the structural parameters should be considered in the analysis. Uncertainties can be represented through random variables described by adequate Probability Distribution Functions (PDFs). For the statistical definition, the distribution type and its parameters might

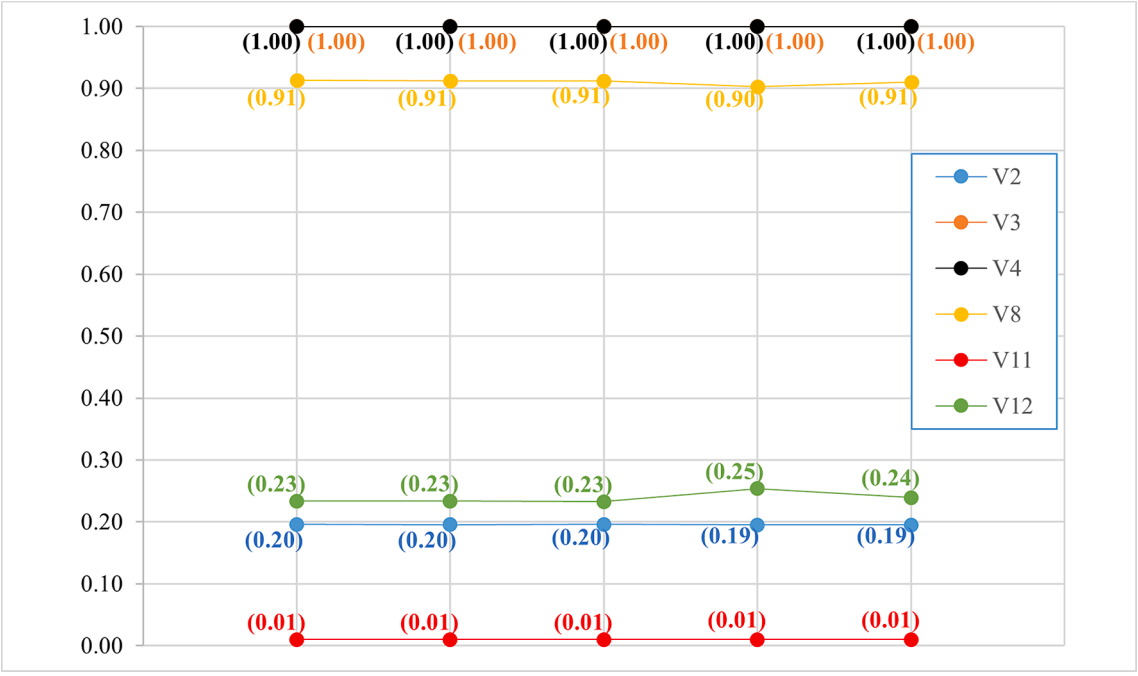

Fig. 16. Normalized values of the calibration parameters for the different genetic algorithm runs.

Table 6
Results obtained after FE model updating.

Mode	Experimental	Calibrated model			Mass participation factors (%)		
	Frequencies (Hz)	Frequencies (Hz)	Error (%)	MAC	UY	UZ	ROTX
1	1.05	1.07	1.72	0.97	0.00	77.36	13.25
2	2.71	2.81	3.37	0.90	0.00	4.81	6.29
3	6.19	6.26	1.17	0.94	70.67	0.00	0.00
4	7.36	7.22	1.90	0.96	0.00	0.00	15.07

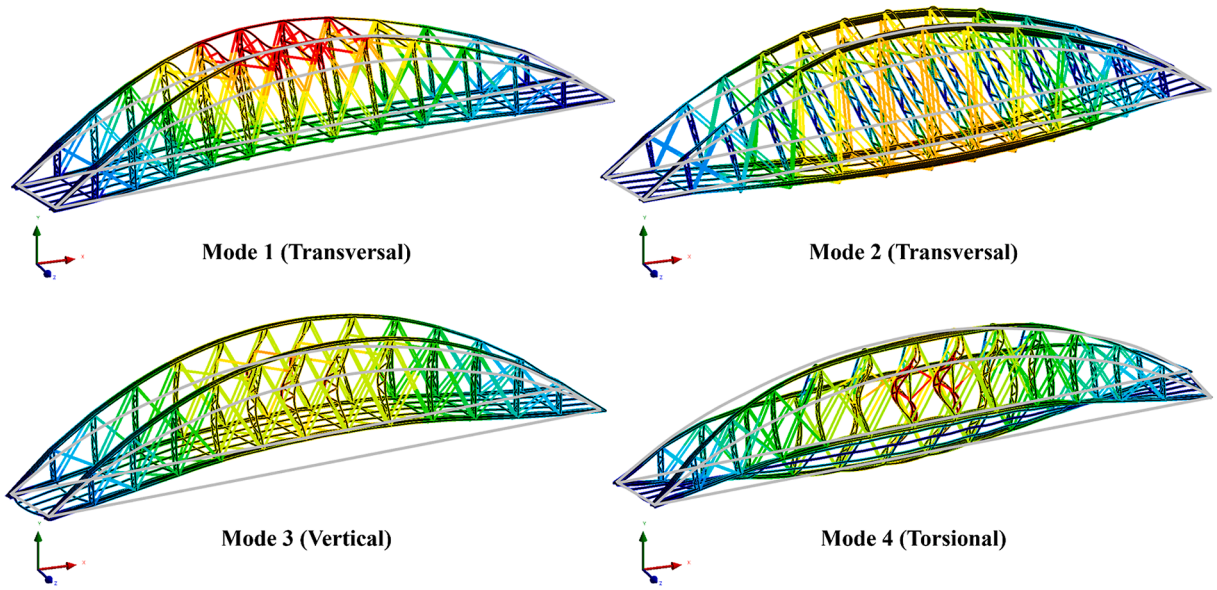

Fig. 17. Numerical mode shapes after model calibration.

be established according to the recommendations provided in the existing literature and the available experimental data.

In this study, for the structural variables considered during the model updating process, the mean value was defined as the corresponding calibrated value, while, for the non-calibrated parameters, the mean value was set to the initial value. Following the recommendations of the Probabilistic Model Code [31], the probability distribution of the Young's modulus was defined as log-normal with a CoV of 3 %, while for the density, a normal distribution with a CoV of 1 % was adopted. The yield strength of the material was characterized as a log-normal distribution with a CoV of 10 % [37]. Regarding the thicknesses of the steel members (see Fig. 4), since corrosion is a complex phenomenon that may involve different material losses from one area to another, the scatter was represented by a normal PDF with a CoV of 5 % [38,39]. Finally, since there is uncertainty in the connections and bearing supports response under high-intensity loads such as traffic actions, this aspect was considered in the assessment process. Thus, triangular distributions using the calibrated value as mode value and previous lower and upper bounds (Section 5.2.1), which, e.g., in the case of steel connections, transform them into pinned or almost fully rigid, were used for modeling the stiffness of steel connections and bridge supports. Table 7 summarizes all considered random variables.

On the other hand, the LM1 load model corresponding to roadway traffic was adopted according to EN 1991–2 [40] to assess the bridge mechanical performance. The LM1 load model divides the deck into virtual lanes according to its width. O Barqueiro Bridge has a width lower than 5.40 m. Hence the deck is divided into a centered virtual lane of 3.00 m width, where a distributed load of 9.00 kN/m^2 is applied, and two remaining areas that withstand a load of 2.50 kN/m^2 each. Moreover, on the virtual lane, four loads of 150 kN each are considered, representing the wheels of a heavy truck acting at the vertices of a

Table 7
Uncertain structural parameters of the numerical model of O Barqueiro bridge.

ID	Parameter	Distribution type	μ	σ
V1	Density	Normal	7850 kg/m^3	78.5 kg/m^3
V2	Young's modulus	Log-normal	184 GPa	5.52 GPa
V3	Arch/girder flange thickness	Normal	17.67 mm	0.88 mm
V4	Arch/girder L-shaped profile thickness	Normal	10.73 mm	0.54 mm
V5	Vertical hanger plate thickness	Normal	8.98 mm	0.45 mm
V6	Vertical hanger L-shaped profile thickness	Normal	8.20 mm	0.41 mm
V7	Stringer L-shaped profile thickness	Normal	7.23 mm	0.36 mm
V8	Crossbeam L-shaped profile thickness	Normal	10.83 mm	0.54 mm
V9	Reinforcement plate thickness	Normal	7.50 mm	0.38 mm
V10	Rotational stiffness of slightly damaged connections	Triangular	6.37E + 06 N•m/rad	2.26E + 06 N•m/rad
V11	Translational stiffnesses of Vicedo support (Y-axis)	Triangular	5.01E + 10 N/m	2.04E + 10 N/m
V12	Translational stiffnesses of O Mañón support (Y-axis)	Triangular	5.01E + 10 N/m	2.04E + 10 N/m
V13	Translational stiffnesses of Vicedo support (Z-axis)	Triangular	3.35E + 07 N/m	2.35E + 07 N/m
V14	Translational stiffnesses of O Mañón support (Z-axis)	Triangular	4.14E + 07 N/m	2.13E + 07 N/m
V15	Steel yield strength	Log-normal	310.05 MPa	31.01 MPa

rectangle of 1.20 in length and 2.00 m in width. For the probabilistic analyses, the uncertainties related to the concentrated and distributed load values of the LM1 loading scheme were modeled, considering a 95th percentile and a return period of 50 years, by means of a Gumbel distribution with a CoV of 15 %, as suggested in [24]. The resultant loading PDFs are shown in Table 8.

6.2. Bayesian inference

Previous probability distributions were defined according to the model updating results, data from the literature, experience, and engineering judgment. Nevertheless, additional observations or experimental results were obtained during the characterization campaign. Thus, Bayesian inference can be adopted to update the previously defined PDFs (prior distributions) considering these additional sources of information, reducing the statistical uncertainty of the random variables' parameters. This updating process is based on the Bayes theorem, which weights the prior distributions and the experimental data (likelihood) to yield the posterior distributions.

It should be noted that not all the prior distributions of Table 7 were updated. Only experimental measurements of the Young's modulus and thicknesses of arches, vertical hangers, crossbeams, stringers, and reinforcement plates were obtained during the in-situ surveys. Hence, only the PDFs related to these structural parameters were updated using Bayesian inference.

In this study, a normal likelihood and conjugate prior distributions were used. On the one hand, the assumption that the data follows a normal distribution was appropriately verified by a hypothesis testing procedure, particularly by the Chi-Square Goodness-of-Fit and the Anderson-Darling tests. On the other hand, informative prior distributions allow for considering existing previous information, particularly regarding the calibrated structural parameters.

The adopted Bayesian framework is described in the following for the case when both moments μ and σ^2 are unknown. For the sake of conciseness, it is exemplified with an application to the arch/girder flange thickness (see Table 7). In the case of the Young's modulus, which follows a log-normal distribution, the logarithmic transformation of the data is first accomplished, and then the same Bayesian analysis is applied.

The conjugate prior of a normal distribution with unknown mean and variance is a normal-inverse-gamma distribution:

$$p(\mu,\sigma^2)\ NIG\left(\mu_0;\frac{\sigma^2}{n_0};\frac{v_0}{2};\frac{v_0}{2}\sigma_0^2\right) \tag{8}$$

where n_0, μ_0, σ_0^2, and $v_0 = n_0 - 1$ are the prior sample size, mean, variance, and degrees of freedom, respectively. In this case, $n_0 = 20$ (the same weight is given to the prior and the likelihood data), $\mu_0 = 17.67$, and $\sigma_0^2 = 0.77$.

The joint prior density can also be expressed as the product of a conditional probability and a marginal probability in the form:

$$p(\mu,\sigma^2) = p(\mu|\sigma^2)p(\sigma^2) \tag{9}$$

where $p(\mu|\sigma^2)$ the prior conditional distribution of μ given σ^2 is a normal PDF with mean μ_0 and variance σ^2/n_0:

$$\mu|\sigma^2\ N\left(\mu_0;\frac{\sigma^2}{n_0}\right)\Rightarrow\mu|\sigma^2\ N\left(17.67;\frac{\sigma^2}{20}\right) \tag{10}$$

and $p(\sigma^2)$ the marginal prior distribution of σ^2 is an inverse gamma distribution with shape $\alpha_0 = v_0/2$ and scale $\beta_0 = \frac{v_0}{2}\sigma_0^2$:

$$\sigma^2\ IG(\alpha_0,\beta_0)\Rightarrow\sigma^2\ IG(9.50,7.36) \tag{11}$$

After seeing the data, $y = \{y_1,\cdots,y_n\}$, in this case with numerical summaries $\bar{y} = 17.67$ (sample mean), $s^2 = 0.24$ (sample variance), and $n = 20$ (number of test results), the conditional posterior distribution of μ given σ^2 is also a normal PDF with mean μ_n and variance σ^2/n_n:

$$\mu|\sigma^2,y\ N\left(\mu_n;\frac{\sigma^2}{n_n}\right)\Rightarrow\mu|\sigma^2,y\ N\left(17.67;\frac{\sigma^2}{40}\right) \tag{12}$$

where.

$$\mu_n = \frac{n_0}{n_0+n}\mu_0 + \frac{n}{n_0+n}\bar{y}$$

$$n_n = n_0 + n$$

It can be noticed that the parameters of the posterior distribution combine the prior information and the one contained in the data. In this regard, μ_n is a weighted average of the prior μ_0 and the sample mean $\bar{y}$, with weights determined by the relative precision of the two pieces of information [41].

The marginal posterior distribution of σ^2 is an inverse gamma PDF with updated hyperparameters $\alpha_n = v_n/2$ and $\beta_n = \frac{v_n}{2}\sigma_n^2$,

$$\sigma^2|y\ IG(\alpha_n,\beta_n)\Rightarrow\sigma^2|y\ IG(19.50,9.64) \tag{13}$$

where:

$$v_n = v_0 + n$$

$$v_n\sigma_n^2 = v_0\sigma_0^2 + (n-1)\bullet s^2 + \frac{n_0\bullet n}{n_0+n}(\bar{y}-\mu_0)^2 \tag{14}$$

Thus, the posterior sum of squares $v_n\sigma_n^2$, combines the prior and the sample sum of squares, $v_0\sigma_0^2$ and $(n-1)\bullet s^2$ respectively, with the additional uncertainty given by the difference between the sample and the prior mean [41]. In order to compute the posterior distribution of the parameters, either simulation methods using Equations (12) and (13) or analytical expressions can be used [41].

For the considered random variable (arch/girder flange thickness), Table 9 provides the results for the posterior distributions obtained from the Bayesian inference analysis. Fig. 18 shows, together with the prior distribution and the likelihood function, a plot of the resulting posterior distribution of the population. Table 10 summarizes the distribution types and corresponding statistical moments of all structural parameters considered for the reliability analysis.

6.3. Deterministic analysis

The load model LM1 is adequate for both local and global

Table 8
LM1 load model distribution type and statistical moments.

ID	Parameter	Distribution type	μ	σ
Q	Force per wheel	Gumbel	117.20 kN	17.58 kN
q_{NL}	Virtual lane distributed load	Gumbel	7.03 kN/m^2	1.05 kN/m^2
q_{RA}	Remaining area distributed load	Gumbel	1.96 kN/m^2	0.29 kN/m^2

Table 9
Posterior distribution parameters values for the arch/girder flange thickness.

Parameter	Posterior
μ_0	17.67 mm
σ_0	0.88 mm
μ	17.67 mm
$\sigma(\mu)$	0.11 mm
σ	0.72 mm
$\sigma(\sigma)$	0.08 mm
μ_{pop}	17.67 mm
σ_{pop}	0.73 mm

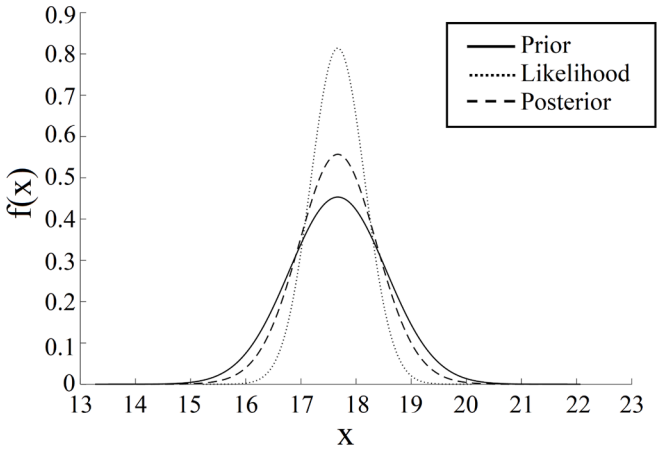

Fig. 18. Prior and posterior probability density functions after Bayesian inference (arch flange thickness).

Table 10
Random variables considered in the reliability analysis.

ID	Parameter	Distribution type	μ	σ
V1	Density	Normal	7850 kg/m^3	78.5 kg/m^3
V2	Young's modulus	Log-normal	187 GPa	8.25 GPa
V3	Arch/girder flange thickness	Normal	17.67 mm	0.73 mm
V4	Arch/girder L-shaped profile thickness	Normal	10.66 mm	0.73 mm
V5	Vertical hanger plate thickness	Normal	9.06 mm	0.89 mm
V6	Vertical hanger L-shaped profile thickness	Normal	8.16 mm	0.66 mm
V7	Stringer L-shaped profile thickness	Normal	7.19 mm	0.99 mm
V8	Crossbeam L-shaped profile thickness	Normal	10.86 mm	0.60 mm
V9	Reinforcement plate thickness	Normal	7.50 mm	0.69 mm
V10	Rotational stiffness of slightly damaged connections	Triangular	6.37E + 06 N•m/rad	2.26E + 06 N•m/rad
V11	Translational stiffnesses of Vicedo support (Y-axis)	Triangular	5.01E + 10 N/m	2.04E + 10 N/m
V12	Translational stiffnesses of O Mañón support (Y-axis)	Triangular	5.01E + 10 N/m	2.04E + 10 N/m
V13	Translational stiffnesses of Vicedo support (Z-axis)	Triangular	3.35E + 07 N/m	2.35E + 07 N/m
V14	Translational stiffnesses of O Mañón support (Z-axis)	Triangular	4.14E + 07 N/mm	2.13E + 07 N/m
V15	Steel yield strength	Log-normal	310.05 MPa	31.01 MPa

verifications. However, EN 1991-2 [40] states that the location of the loads must be previously chosen to guarantee the most unfavorable effects. Accordingly, a deterministic analysis, adopting the mean values of the random parameters, was first performed to identify the most critical section of the bridge. Thus, a total of twenty different loading cases were defined along the span length of the structure.

In each position, a non-linear static analysis was performed to calculate the failure load factor. Geometric and material non-linearity effects were taken into account. The plastic behavior of the steel was described by the von Mises yield criteria with an isotropic hardening assumption [42]. For the non-linear analysis, a two-load-step procedure was followed. In the first step, the self-weight of the structure was introduced, mobilizing the stress-stiffening response of the tension-only truss elements. In the second step, using the achieved equilibrium state as a starting point, the LM1 live loading was monotonically increased up to the bridge failure. To solve the non-linear problem, the incremental-iterative full Newton-Raphson method with a convergence criterion based on forces and displacements was adopted.

The results per loading position are indicated in Fig. 19. In this figure, an asymmetry in the failure load factor results can be noticed. These deviations can be attributed to the damaged condition of the steel connections involving the tie girders, vertical hangers, and crossbeams. For the critical loading scenario (sixth position), the failure mechanism of the bridge is shown in Fig. 20. The failure is triggered in the stringer positioned in the middle of the load model application. The live loads deform this structural element until a hinged mechanism is formed, leading to a flexural failure. No significant bending moments are transferred to the connected crossbeams despite the appreciable bending of the stringer. This is due to the action of the beam-end releases, which mimic the actual steel connections, allowing free in-plane rotations.

The obtained failure load factors seem to indicate that the roadway traffic can not safely cross the bridge. Nevertheless, reliability analysis, which explicitly considers the parameter values uncertainty, should be used to compute the ultimate load-carrying capacity more accurately. This way, a more reliable judgment about the actual safety condition of the bridge can be emitted.

6.4. Reliability analysis

Any structure must fulfill certain requirements during specific service conditions and lifetime. The concept of limit state delimits these requirements, so if this is surpassed, the structure will no longer fulfill them. The limit states can be referred to stability and strength requirements (Ultimate Limit State) or the functionality and serviceability of the construction (Serviceability Limit State). For instance, in the case of an Ultimate Limit State (ULS), this can be expressed as a function comparing the resistance and the effects of loads:

$$g(\boldsymbol{X}) = R - S \tag{15}$$

where $g(\boldsymbol{X})$ is the limit state function, $\boldsymbol{X}$ is a vector of random variables, R refers to the resistance, and S denotes the effect of loads. Accordingly, the probability of failure p_f can be defined as the probability that the structure has not enough resistance to withstand the applied loads. Thus, it can be expressed as:

$$p_f = P(g(\boldsymbol{X}) \leq 0) = P(R - S \leq 0) = P(R \leq S) \tag{16}$$

An alternative indicator, the reliability index β, can be calculated using the failure probability [43], which denotes the reliability level of the structure:

$$\beta = -\Phi^{-1}(p_f) \tag{17}$$

where $\Phi(\bullet)$ is the standard normal cumulative distribution function. In order to assess bridge safety, the reliability index is compared with the target values established in the current standards.

6.4.1. Serviceability limit state

In the current standards [44,45], the serviceability limit state is referred to the loss of usability of the structure in a normal condition. There are several usability indicators, but in this study, the existence of local damage that affects the structure's appearance, efficacy, or functionality was chosen. Equation (18) describes the selected serviceability limit state, where σ_{VMmax} is the maximum Von Mises stress and f_y denotes the yield strength of the material. This limit state assesses if some element of the construction surpasses the yield strength of the material entering into the inelastic domain. As a reliability algorithm, the Directional Sampling (DS) method [46] was chosen. A total of 200 directions were analyzed to perform the probabilistic analysis. The obtained results are indicated in Table 11.

$$\sigma_{VMmax} \leq f_y \tag{18}$$

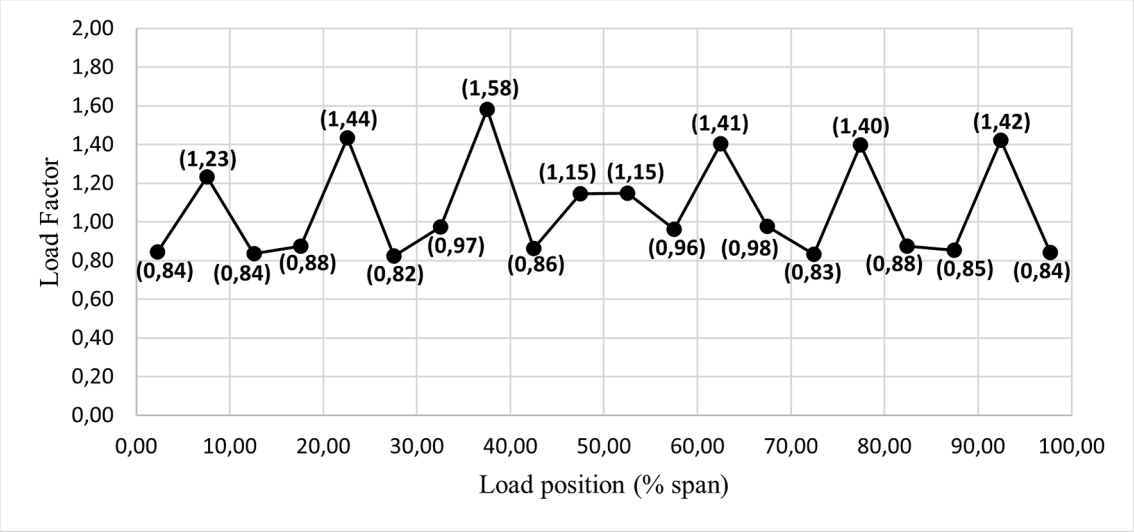

Fig. 19. Failure load factors for the different loading positions along the span length of the bridge in the deterministic analysis.

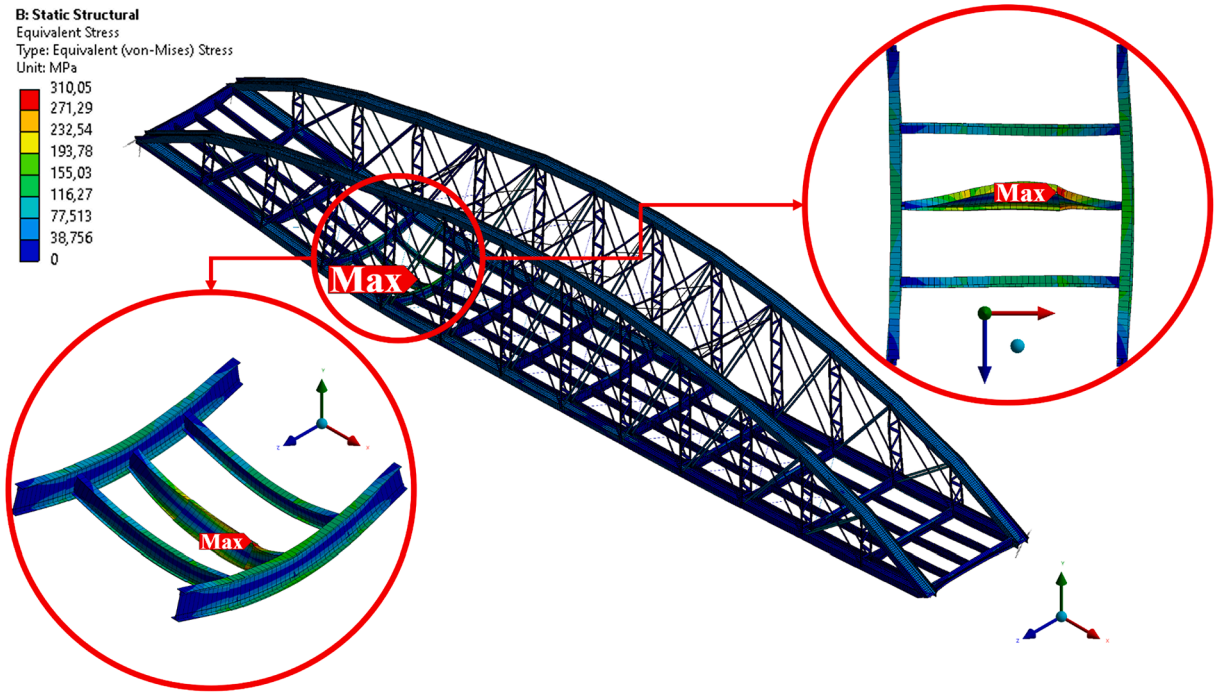

Fig. 20. Detail of the bridge failure mechanism for the critical loading position.

Table 11
Reliability analysis results for the serviceability limit state.

Probability of failure	0.04
Reliability index	1.80

The calculated reliability index must be compared with the target values established in the current standards for assessing the structure's performance. Four standards were studied: the UNE-EN 1990 [44], ISO 2394 [47], ISO 13,822 [48], and the JCSS [49], which present several differences between them. The UNE-EN 1990 and the JCSS are referred to the design of new structures, while the ISO 2394 and the ISO 13,822 establish target reliability indexes for existing structures. ISO 2394 states that the target reliability indexes should be the same for existing and new structures, while ISO 13,822 points out that it cannot be possible because of economic, social, and sustainability considerations such as the incremental costs in structural upgrading or the "minimum structural intervention" requirement. The JCSS standard agrees with ISO 13,822 and states that target reliability indexes for existing structures should be lower than for new structures.

Besides, each standard is referred to a particular reference period. UNE-EN 1990 specifies different target reliability indexes for a one-year or a fifty-year reference period, while the ISO 2394 and the JCSS only consider a reference period of one year. On the other hand, ISO 13,822 provides target reliability indexes referred to the minimum standard period for safety (e.g., 50 years) concerning the ultimate limit states and the intended remaining service life if a serviceability limit state is considered.

Finally, each standard indicates its target indexes using different approaches. In UNE-EN 1990, they depend on the consequence class of the structure, which classifies the construction under study regarding the economic, social, environmental, and living costs that the structure will generate if it collapses. In ISO 2394, the indices are established using the Life Quality Index (LQI), which measures society's predisposition to invest in health and life safety improvement. This is calculated by the life expectancy, the per capita Gross Domestic Product and the ratio between working and leisure time of a country. The LQI leads to calculating the life-saving costs, which are the affordable and necessary costs that must be invested to save one additional life. On the other hand, the target reliability indices of ISO 13,822 are based on ISO 2394. Moreover, their serviceability target limit states are classified by identifying if the failure is reversible or not. Finally, the JCSS standard indicates its serviceability target indices like the previous standard.

In this study, O Barqueiro bridge has been classified as a structure with moderate consequences of failure because its deck is not wide enough for several vehicles to cross simultaneously and due to the existence of additional bridges near it which offer an alternative route. Concerning the life savings and safety costs, the bridge has already surpassed the design service life established in the standards (100 years), which will increase the expenses required for achieving a higher reliability index. Therefore, its life-saving and safety costs should be the highest specified in the standards. Table 12 compares the calculated serviceability and target reliability indexes indicated in the standards. All requirements are fulfilled except for a one-year reference period in the UNE-EN 1990 standard ($\beta_t = 2.90$).

6.4.2. Ultimate limit state

Ultimate limit states are related to the safety of the structure and its users. In this study, the failure due to the transformation of the structure, or part of it, into a mechanism that leads to collapse has been evaluated. Hence, the ultimate load-carrying capacity of the bridge was assessed (see Equation (15)) by means of non-linear structural analysis. As a reliability algorithm, the Directional Sampling method was used, and the obtained results (i.e., failure probability and reliability index) are shown in Table 13.

Regarding the safety assessment, the ISO 13,822 and the JCSS standards establish their target reliability indices according to the consequences of failure, similar to the UNE-EN 1990. Moreover, the JCSS states that failure's consequences also depend on the type of failure (e.g., a structure that can collapse suddenly should be classified as a structure with large consequences of failure). Table 14 shows the bridge safety assessment according to the studied standards.

The results indicate that the O Barqueiro bridge does not present satisfactory structural performance to withstand the roadway traffic loads safely. Therefore, it is recommended to keep the crossing limited to pedestrians. These results agree with the conclusions extracted from the visual inspection. The structure presents severe corrosion damage in some local areas, such as the steel connections, and this damage impacts its ultimate strength. Hence, to put the construction back in service, appropriate rehabilitation works should need to be undertaken.

7. Conclusions

In this paper, a holistic methodology for the non-destructive experimental characterization and reliability-based structural assessment of historical steel bridges was presented. The methodology comprehends all the critical stages for adequately assessing the structural system performance (i.e., experimental characterization, numerical modeling, finite element model updating, and probabilistic-based structural analysis). An aging riveted steel arch bridge in Galicia, northwest Spain, was considered to validate the feasibility of the methodology. The following conclusions can be drawn from the study:

- In order to characterize ancient steel bridges effectively at multiple levels: geometry, material, and structural system, especially for those presenting signs of degradation and deterioration, a comprehensive experimental characterization is needed. The synergetic combination of several non-destructive testing techniques such as terrestrial laser scanning, ultrasonic testing, and operational modal analysis is an effective approach while preserving the non-intrusion requirement regarding heritage constructions.
- Sensor data can be further complemented with more conventional visual inspections and on-site measurements to gather broader information exploited throughout the assessment procedure, i.e., during the finite element model development, the model calibration process, and the structural reliability analysis.
- Combining a sample-based global sensitivity analysis (e.g., Spearman correlation coefficients) with a global optimization method (e.g., genetic algorithm) using a response surface approximation (e.g., Douglas-Reid approach) is a cost-effective solution for finite element model updating based on vibration data balancing accuracy and computational effort suitably. In this study, based on a space-filling set of 600 model runs, the whole process was accomplished, obtaining a calibrated model with an average relative error in frequencies of 2.04 % and an average MAC value of 0.94.
- A reliability-based structural analysis framework is a suitable approach for explicitly considering uncertainty in the safety assessment process, where the prior probabilistic model is defined according to information from literature and FE model updating results and then further updated on the basis of the results of the in-situ tests (e.g., ultrasonic testing and geometric measurements) using Bayesian inference procedures.
- The proposed methodology allows the systematic model calibration, updating of the parameters' probability distributions, and reassessment of the structural system performance as new experimental data is gathered. Hence, adequate tracking of the structural safety level over time can be addressed.
- Concerning the case study (O Barqueiro Bridge), at present, comparing the obtained reliability indexes with the target values established in the current standards allows us to conclude that the bridge does not present satisfactory structural performance. Hence, the passage of loads related to road traffic should be seen as exceptional; otherwise, structural upgrading is necessary.

Table 12
Serviceability assessment of O Barqueiro bridge according to the target values of the reliability index.

Standard	Target reliability index (β_t)	Reliability index (β)	
UNE-EN 1990	1.50	1.80	☐
ISO 13822	1.50		☐
JCSS	1.30		☐

Table 13
Reliability analysis results for the ultimate limit state.

Probability of failure	0.02
Reliability index	1.99

Table 14
Structural safety assessment of O Barqueiro bridge according to the target values of the reliability index.

Standard	Target reliability index (β_t)	Reliability index (β)	
UNE-EN 1990	3.80	1.99	×
ISO 2394	3.10		×
ISO 13822	3.80		×
JCSS	3.30		×

Future methodology improvements will be focused on jointly using static (e.g., load tests displacements) and dynamic (e.g., modal properties) responses for improved parameter identification targeted to response prediction in failure regions. Future works will also evaluate complementing the battery of non-destructive testing methods with additional techniques such as hardness testing that might be useful for obtaining the ultimate strength of steel.

CRediT authorship contribution statement

O. Bouzas: Methodology, Software, Investigation, Writing – original draft. **B. Conde:** Conceptualization, Validation, Writing – review & editing. **M. Cabaleiro:** Methodology, Investigation, Resources. **B. Riveiro:** Supervision, Funding acquisition.

Declaration of Competing Interest

The authors declare that they have no known competing financial interests or personal relationships that could have appeared to influence the work reported in this paper.

Data availability

The authors do not have permission to share data.

Acknowledgements

This work has been partially supported by the Spanish Ministry of Science, Innovation, and Universities through the project Ref. RTI2018-095893-B-C21, and the SIRMA project, co-financed by the INTERREG Atlantic Area Programme through the European Regional Development Fund (ERDF) with application code: EAPA_826/2018. Work produced with the support of a 2021 Leonardo Grant for Researchers and Cultural Creators, BBVA Foundation. The BBVA Foundation takes no responsibility for the opinions, statements and contents of this project, which are entirely the responsibility of its authors. Funding for open access charge: Universidade de Vigo/CISUG.

References

[1] ISCARSAH (International Scientific Committee for Analysis and Restoration of Structures of Architectural Heritage). Recommendations for the analysis, conservation and structural restoration of Architectural Heritage; 2003.
[2] Anigacz W, Beben D, Kwiatkowski J. Hybrid measurement techniques used to a study of historic cast iron suspension bridge. In: IOP conference series: materials science and engineering, vol. 419. Institute of Physics Publishing; 2018. doi: 10.1088/1757-899X/419/1/012013.
[3] Riveiro B, Morer P, Arias P, de Arteaga I. Terrestrial laser scanning and limit analysis of masonry arch bridges. Constr Build Mater 2011;25(4):1726–35. https://doi.org/10.1016/j.conbuildmat.2010.11.094.
[4] Kim D, Kwak Y, Sohn H. Accelerated cable-stayed bridge construction using terrestrial laser scanning. Autom Constr 2020;117:103269. https://doi.org/10.1016/j.autcon.2020.103269.
[5] Yan Y, Hajjar JF. Automated extraction of structural elements in steel girder bridges from laser point clouds. Autom Constr 2021;125:103582. https://doi.org/10.1016/j.autcon.2021.103582.
[6] Gyetvai N, Truong-Hong L, Laefer DF. Laser scan-based structural assessment of wrought iron bridges: Guinness Bridge, Ireland. Proc Inst Civil Eng - Eng History Heritage 2018;171(2):76–89.
[7] Krautkrämer J, Krautkrämer H. Ultrasonic testing of materials. Springer Berlin Heidelberg; 1990. doi: 10.1007/978-3-662-10680-8.
[8] Costa BJA, Magalhães F, Cunha Á, Figueiras J. Rehabilitation assessment of a centenary steel bridge based on modal analysis. Eng Struct 2013;56:260–72. https://doi.org/10.1016/j.engstruct.2013.05.010.
[9] Marques F, Moutinho C, Magalhães F, Caetano E, Cunha Á. Analysis of dynamic and fatigue effects in an old metallic riveted bridge. J Constr Steel Res 2014;99:85–101. https://doi.org/10.1016/j.jcsr.2014.04.010.
[10] Altunişik AC, Karahasan OŞ, Genç AF, Okur FY, Günaydin M, Adanur S. Sensitivity-based model updating of building frames using modal test data. KSCE J Civ Eng 2018;22(10):4038–46. https://doi.org/10.1007/s12205-018-1601-6.
[11] Altunişik AC, Okur FY, Genç AF, Günaydin M, Adanur S. Automated model updating of historical masonry structures based on ambient vibration measurements. J Perform Constr Facil 2018;32(1).
[12] Yang YB, Chen YJ. A new direct method for updating structural models based on measured modal data. Eng Struct 2009;31(1):32–42. https://doi.org/10.1016/j.engstruct.2008.07.011.
[13] Ribeiro D, Calçada R, Delgado R, Brehm M, Zabel V. Finite element model updating of a bowstring-arch railway bridge based on experimental modal parameters. Eng Struct 2012;40:413–35. https://doi.org/10.1016/j.engstruct.2012.03.013.
[14] Malveiro J, Ribeiro D, Sousa C, Calçada R. Model updating of a dynamic model of a composite steel-concrete railway viaduct based on experimental tests. Eng Struct 2018;164:40–52. https://doi.org/10.1016/j.engstruct.2018.02.057.
[15] Bautista-De Castro Á, Sánchez-Aparicio LJ, Ramos LF, Sena-Cruz J, González-Aguilera D. Integrating geomatic approaches, Operational Modal Analysis, advanced numerical and updating methods to evaluate the current safety conditions of the historical Bôco Bridge. Constr Build Mater 2018;158:961–84. https://doi.org/10.1016/j.conbuildmat.2017.10.084.
[16] Conde B, Ramos LF, Oliveira DV, Riveiro B, Solla M. Structural assessment of masonry arch bridges by combination of non-destructive testing techniques and three-dimensional numerical modelling: application to Vilanova bridge. Eng Struct 2017;148:621–38. https://doi.org/10.1016/j.engstruct.2017.07.011.
[17] Wan HP, Ren WX. Stochastic model updating utilizing Bayesian approach and Gaussian process model. Mech Syst Sig Process 2016;70–71:245–68. https://doi.org/10.1016/j.ymssp.2015.08.011.
[18] Cheng J, Li QS. Reliability analysis of a long span steel arch bridge against wind-induced stability failure during construction. J Constr Steel Res 2009;65(3):552–8. https://doi.org/10.1016/j.jcsr.2008.07.019.
[19] Kueres S, Hegger J. Reliability analysis of footbridges pre-tensioned with carbon fiber reinforced polymer tendons under flexural loading. Eng Struct 2020;203:109546. https://doi.org/10.1016/j.engstruct.2019.109546.
[20] Jamali S, Chan THT, Nguyen A, Thambiratnam DP. Reliability-based load-carrying capacity assessment of bridges using structural health monitoring and nonlinear analysis. Struct Health Monitoring 2019;18(1):20–34. https://doi.org/10.1177/1475921718808462.
[21] Matos JC, Cruz PJS, Valente IB, Neves LC, Moreira VN. An innovative framework for probabilistic-based structural assessment with an application to existing reinforced concrete structures. Eng Struct 2016;111:552–64. https://doi.org/10.1016/j.engstruct.2015.12.040.
[22] Moreira VN, Fernandes J, Matos JC, Oliveira D v. Reliability-based assessment of existing masonry arch railway bridges. Constr Build Mater 2016;115:544–54. doi: 10.1016/j.conbuildmat.2016.04.030.
[23] Moreira VN, Matos JC, Oliveira Dv. Probabilistic-based assessment of a masonry arch bridge considering inferential procedures. Eng Struct 2017;134:61–73. doi: 10.1016/j.engstruct.2016.11.067.
[24] Conde B, Matos JC, Oliveira Dv, Riveiro B. Probabilistic-based structural assessment of a historic stone arch bridge. Struct Infrastruct Eng 2021;17:379–91. doi: 10.1080/15732479.2020.1752261.
[25] Matos JC, Moreira VN, Valente IB, Cruz PJS, Neves LC, Galvão N. Probabilistic-based assessment of existing steel-concrete composite bridges – application to Sousa River Bridge. Eng Struct 2019;181:95–110. https://doi.org/10.1016/j.engstruct.2018.12.006.
[26] Flanigan KA, Lynch JP, Ettouney M. Probabilistic fatigue assessment of monitored railroad bridge components using long-term response data in a reliability framework. Struct Health Monitoring 2020;19(6):2122–42. https://doi.org/10.1177/1475921720915712.
[27] Lubowiecka I, Armesto J, Arias P, Lorenzo H. Historic bridge modelling using laser scanning, ground penetrating radar and finite element methods in the context of structural dynamics. Eng Struct 2009;31(11):2667–76. https://doi.org/10.1016/j.engstruct.2009.06.018.
[28] Altunişik AC, Adanur S, Genç AF, Günaydin M, Okur FY. Non-destructive testing of an ancient Masonry Bastion. J Cult Heritage 2016;22:1049–54. https://doi.org/10.1016/j.culher.2016.05.008.
[29] Pastor M, Binda M, Harčarik T. Modal Assurance Criterion. Procedia Eng 2012;48:543–8.
[30] van Leeuwen R. Cross-Section Analysis in Python; 2017.
[31] Joint Committee on Structural Safety. Probabilistic Model Code. Part 2: Load Models; 2001.
[32] Pang Y, Wu X, Shen G, Yuan W. Seismic fragility analysis of cable-stayed bridges considering different sources of uncertainties. J Bridge Eng 2014;19:04013015. https://doi.org/10.1061/(asce)be.1943-5592.0000565.
[33] European Committee for Standardization. Corrosion of metals and alloys - Corrosivity of atmospheres - Classification, determination and estimation (ISO 9223:2012). Brussels; 2012.
[34] European Committee for Standardization. Corrosion of metals and alloys - Corrosivity of atmospheres - Guiding values for the corrosivity categories (ISO 9224:2012). Brussels; 2012.
[35] Gibbons JD, Chakraborti Subhabrata. Nonparametric statistical inference. Marcel Dekker; 2003.
[36] Zordan T, Briseghella B, Liu T. Finite element model updating of a tied-arch bridge using Douglas-Reid method and Rosenbrock optimization algorithm. J Traffic Transp Eng (English Edition) 2014;1(4):280–92.
[37] Simões da Silva L, Rebelo C, Nethercot D, Marques L, Simões R, Vila Real PMM. Statistical evaluation of the lateral-torsional buckling resistance of steel I-beams, Part 2: Variability of steel properties. J Constr Steel Res 2009;65(4):832–49. https://doi.org/10.1016/j.jcsr.2008.07.017.
[38] Kala Z, Melcher J, Puklický L. Material and geometrical characteristics of structural steels based on statistical analysis of metallurgical products. J Civil Eng Manage 2009;15:299–307. https://doi.org/10.3846/1392-3730.2009.15.299-307.

[39] Arrayago I, Rasmussen KJR, Real E. Statistical analysis of the material, geometrical and imperfection characteristics of structural stainless steels and members. J Constr Steel Res 2020;175:106378. https://doi.org/10.1016/j.jcsr.2020.106378.
[40] European Committee for Standardization. Eurocode 1: Actions on structures. Part 2: Traffic loads on bridges (EN 1991-2). Brussels; 2019.
[41] Gelman A, Carlin JB, Stern HS, Dunson DB, Vehtari A, Rubin DB. Bayesian Data Analysis. third ed. CRC Press; 2014.
[42] European Committee for Standardization. Eurocode 3: Design of steel structures. Part 1-5: Plated structural elements (EN 1993-1-5). Brussels; 2013.
[43] Nowak AS, Collins KR. Reliability of Structures. second ed. CRC Press; 2012.
[44] European Committee for Standardization. Eurocode. Basis of structural design (EN 1990). Brussels; 2019.
[45] European Committee for Standardization. Eurocode 3: Design of steel structures. Part 2: Steel bridges (EN 1993-2). Brussels; 2013.
[46] Dynardo GmbH, Weimar. Methods for multi-disciplinary optimization and robustness analysis; 2019.
[47] International Organization for Standardization. General principles on reliability for structures (ISO 2394:2015); 2015.
[48] International Organization for Standardization. Bases for design of structures - Assessment of existing structures (ISO 13822); 2012.
[49] Joint Committee on Structural Safety. Probabilistic Model Code. Part 1: Basis of design; 2000.